Journal of the European Ceramic Society 42 (2022) 5565–5574

Contents lists available at ScienceDirect

Journal of the European Ceramic Society

journal homepage: www.elsevier.com/locate/jeurceramsoc

Progress towards wafer-scale fabrication based on gel casting technique for 1–3 randomised piezocomposite μUS linear array

A. Boonruang [a,b,*], T. Thongchai [c], Y. Jiang [d], C.E.M. Demore [e], S. Neale [b], A. Moldovan [b], T.W. Button [f], S. Cochran [b]

[a] Expert Centre of Innovative Materials, Thailand Institute of Scientific and Technological Research, Pathum Thani, Thailand
[b] Centre for Medical and Industrial Ultrasonics, James Watt School of Engineering, University of Glasgow, Glasgow, Scotland, UK
[c] Faculty of Engineering, Naresuan University, Phitsanulok, Thailand
[d] NMPA Key Laboratory for Pharmaceutical Excipients Engineering Technology Research, Hunan Institute for Drug Control, Changsha, China
[e] Sunnybrook Research Institute and Department of Medical Biophysics, University of Toronto, Toronto, Canada
[f] School of Metallurgy and Materials, University of Birmingham, UK

ARTICLE INFO

Keywords:
Gel casting
1–3 randomised piezocomposite
Spurious modes
Photolithography
Microultrasound

ABSTRACT

Microultrasound (μUS) linear arrays operating at frequencies over 25 MHz have applications in high resolution biomedical imaging. 1–3 connectively piezoceramic – polymer composite ("piezocomposite") material is attractive for fabrication of these devices due to its high effective electromechanical coupling coefficient and low acoustic impedance for better acoustic matching between transducer and tissue. However, a major concern with this type of material comes from interference between the fundamental thickness-mode resonance and spurious modes, which is usually generated by wave propagation and reflection within the repetitive and symmetrical structure of classical piezocomposite. In general, a fine spatial scale is required of the material structure to suppress the spurious modes; however, the fabrication process is challenging using standard dice-and-fill methods at the fine scales required for high frequencies. A promising way to overcome this challenge is to manipulate the lateral geometry and spacing of the piezoceramic pillars with a random distribution. In this work, gel casting in association with a micromoulding technique has been developed for manufacturing 1–3 randomised piezocomposite active material for μUS linear arrays. 48 vol% solid loading of piezoceramic powder with 30 wt% Hydantoin resin content was employed to prepare a low viscosity aqueous suspension. Through varying powder size, it was found that the suspension with 1.22 μm powder had the highest viscosity, ~ 0.47 Pa.s, and a short gelation time, ~ 10 mins. However, all suspensions had viscosities less than 1 Pa.s at a shear rate of 100 s^{-1}, indicating that they had good flowability. The green body samples showed mean flexural strength 49.7 ± 2.49 MPa. After piezocomposite fabrication with randomised pillars, surface planarisation was used to obtain reliable edge definition of photolithographically-defined electrodes. 20-element arrays with 50-μm element pitch were configured using a bilayer lift-off process. The 1–3 randomised piezocomposite demonstrated its capability to minimise the effects of spurious modes in the thickness mode frequency range, while the thickness resonances provided $k_{33} = 0.67$. Without a matching layer, the array produced a − 6 dB bandwidth of 38.4%- and − 20-dB pulse length of 0.26 μs. These results show that 1–3 randomised piezocomposite fabricated from gel-casting associated with a micromoulding technique is feasible for fabrication of μUS linear arrays and may offer a route to small wafer-scale production.

1. Introduction

Microultrasound arrays based on 1–3 connectivity piezoceramic – polymer composite ("piezocomposite") material are attractive for use in many research domains since the material possesses electromechanical and acoustic properties that are better than bulk piezoelectric materials. For instance, piezocomposites provide improved electromechanical coupling coefficients in thickness modes (k_t ~ *0.6–0.75*), leading to increased operating bandwidth and sensitivity [1,2], and lower acoustic impedance (Z_a ~ *7.5 – 15 MRayl*) which is associated with better

* Corresponding author at: Expert Centre of Innovative Materials, Thailand Institute of Scientific and Technological Research, Pathum Thani, Thailand.
E-mail address: arjin@tistr.or.th (A. Boonruang).

https://doi.org/10.1016/j.jeurceramsoc.2022.05.061
Received 7 November 2021; Received in revised form 20 May 2022; Accepted 24 May 2022
Available online 26 May 2022

acoustic matching between the transducer and the medium in which the ultrasound propagates [2,3].

However, an inherent hindrance of piezocomposite with the repetitive and symmetrical structure usually realized in 1–3 connectivity materials is the generation of spurious modes. These modes arise from waves propagating in the lateral direction between pillars and reflected at the parallel pillar faces within the composite structure [4]. They are accentuated in μUS transducers operating at high frequencies, with the spurious resonances closer to the fundamental thickness resonances. This is because it is difficult to fabricate piezocomposite with the pillar width and spacing sufficiently different from the thickness [4]. In consequence, the spurious modes are coupled with the thickness mode of the transducer, which leads to degradation in transducer performance and image quality [5].

The spurious modes can be minimised by strategies based on enhancement of the fundamental thickness resonances to be dominant over them. This can ideally be achieved by minimising the width of the piezoelectric pillars to ensure the aspect ratio (*AR*), i.e. the pillar height-to-width ratio, is greater than three [4,6]. Another approach is to use soft setting polymers as the passive phase of the composite. The viscosity of the soft epoxy greatly damps the laterally-propagating spurious modes, which leads to an improvement in the thickness mode operation [7,8]. Problems with this approach, however, are the high viscosity of the soft epoxy prior to curing and its softness post-cure, which cause many difficulties during the fabrication process e.g., filling, machining, surface finishing and poling [8,9].

Another method relies on increasing the level of geometrical complexity in the piezocomposite structure [10–12]. This concept demonstrated its capability to push the spurious modes beyond the thickness mode operating frequency because the uneven distribution of the pillar faces reduces the laterally propagating energy. In 2009, a novel arbitrary design, namely a randomised pattern, achieved by manipulating the pillar cross-sectional geometries, dimensions and separations was developed and proposed by Démoré et al. [13]. Finite element analysis of this composite pattern with feature sizes in the range 2–50 μm suggested that it could effectively eliminate the spurious modes by spreading them over a broad frequency range, while maintaining the fundamental thickness mode for functional performance of the μUS transducers.

Unfortunately, microscale piezocomposites with geometrically complex pillars are difficult or impossible to fabricate with a standard dice-and-fill method [10–12], injection moulding [14,15], interdigital pair bonding (IPB) [16,17], laser micromachining [18–20], lost Si mould [21], and viscous polymer processing (VPP) [22,23]. This is because each of these methods has its own limitations, such as: difficulty in producing fine kerfs below 10 μm through the dice-and-fill method, poor *AR* of the composite structure and time-consuming process in IPB, high-production costs in injection moulding and laser micromachining, chemical contamination in the lost mould process, and high viscosity paste in VPP that is unable to produce the complex shape pillars. To overcome these difficulties, gel casting (GC) is proposed and demonstrated in this paper for fabricating ultra-fine scale 1–3 randomised piezocomposites for high frequency single element transducer (SETs) [24] and arrays. It is confirmed that the piezocomposite that is obtained has an isolated thickness mode resonance and spurious mode rejection [24] compared with symmetrical 1–3 piezocomposites [8,10].

2. Gel casting for 1–3 piezocomposite fabrication

The GC method, a near net-shape forming technique, was initially developed in the 1980s by Omatete's team at Oak Ridge National Laboratory (ORNL, TN, USA) to tackle challenges in complex shape forming for advanced ceramic processing [25]. It involves dispersing ceramic powders in a solution containing a monomer, crosslinker, initiator and catalyst to form a relatively low viscosity slurry. The slurry is cast into a mould of the desired shape, in which it becomes the gelling part or the gelation system, with the monomer solution polymerised in-situ and crosslinked to form a strong polymer structure. The dispersed ceramic particles are then held within this three-dimensional (3D) network in the mould.

In the early stages of process development of gel casting, the mechanism of gelation relied on the free radical polymerisation of two monomers, e.g., acrylamide, methacrylamide or n-vinyl pyrrolidone. However, this mechanism cannot be used in air because the free radicals in the monomers react readily with oxygen, producing surface exfoliation of the compacted green sample. Thus, the gelation process must take place in an enclosed chamber, either with high humidity ($>$ 90%) or filled with N_2 inert gas, to minimise the internal stress in the sample and decrease the drying time [26,27]. This introduces high production cost and process complexity. Therefore, self-hardening polymers, comprising thermosetting or water soluble epoxies and hardener, were subsequently applied in the gelling system in order to allow the process to be performed in normal atmospheric conditions [28,29]. The polymerisation of the self-hardening process relies on a nucleophilic addition reaction, which is not inhibited by oxygen in air [29].

In 2012, Jiang et al [24]. reported that it was feasible to merge gel casting with micromoulding to create 1–3 randomised piezocomposites for 30 MHz SETs. The key to this process is the use of high solid loading for high green strength of the fabricated structure whilst retaining a low viscosity in the suspension for good flowability during casting. It was found that a suspension with 45 vol% PZT solid loading and 40 wt% EGDGE (ethylene glycol diglycidyl ether) resin content provided low viscosity, $<$ 2 Pa.s, and relatively high green strength, 35 MPa. However, EGDGE causes irritation to the skin and eyes. Therefore, it was replaced by hydantoin epoxy resin which is nontoxic and highly soluble in water [28,30]. Hydantoin epoxy resin was further used as the monomer in the gelling system. The suspension with 48 vol% PZT solid loading and 30 wt% hydantoin resin content had both lower viscosity, $<$ 1 Pa.s, and provided green samples with higher strength, $\sim$ 48 MPa [30]. The low viscosity potentially aided the slurry to fully fill the complex mould cavities of the randomised pattern, with features with lateral dimensions in the range 2–50 μm. The height of the ceramic pillars was around 140 μm, leading to *AR* up to 70 after demoulding [30].

Research has shown that GC possesses several benefits over the previous methods, i.e., dice-and-fill, IPB, laser machining, and VPP. Firstly, it is highly capable of producing ceramic pillars with ultra-fine dimensions, high *AR*, and complex shape due to the low shear viscosity of the suspension, lower than VPP paste ($\sim 10^5$ Pa.s) [24,31]. Secondly, it provides green body samples with homogeneous microstructure and minimal imperfections. This is because it is based on colloidal processing that can control particle interaction and increase the homogeneity of particle packing in the wet stage. It also provides flexibility in the choice of monomer systems to allow alteration of solid loading with respect to the viscosity of the slurry, resulting in uniform shrinkage and less defects [28]. Thirdly, high flexural strength can be achieved due to high-quality green body samples, allowing the material to withstand demoulding and subsequent processing steps [24]. Additionally, it can provide a low production cost since a reusable master mould can be used to achieve the randomised pattern.

The objective of the work reported in this paper is to demonstrate the development of GC associated with micromoulding to produce 1–3 connectivity randomised piezocomposite μUS arrays which minimise the spurious modes, whilst maintaining the resonance frequencies of the transducer. This method may then be employed to fabricate wafer-scale composites for μUS array applications.

3. Experimental work

3.1. Materials and reagents

A PZT-5H powder (TRS 610C TRS Technologies, PA, USA) with a density of 7.94 g/cm^3 were wet milled by the vibro-milling method for

24, 36 and 39 hr respectively. Suspensions were prepared by adding 250 g powder and 200 g of zirconia balls with 5- and 10-mm diameter into 300 ml of distilled water in a polyethylene bottle and placed in a vibro-milling machine (Model M.18, Sweco Europe S.A., Belgium). After milling the suspensions were freeze dried (Edwards Modulyo Freeze dryer, Labconco Crop., Kansan City, USA). The particle size distribution (PSD) of milled powders was characterised by a laser diffraction particle size analyser (Sympatec, Bury, UK) and specific surface area (SSA) was measured by a Brunauer–Emmett–Teller (BET) analyser (Model ASAP 2010c, Micromeritics, Norcross, USA). The resin system comprised a hydantoin resin (Xitai Chemical, China), soluble in distilled water, with Dispex AA4040 (BASF, Germany) as dispersant, and Bis (3-aminopropyl) amine (Sigma-Aldrich, Germany) as the consolidating agent.

3.2. Suspension preparation and characterisation

48 vol% of PZT solid loading was dispersed in the aqueous solution containing 30 wt% hydantion resin and other additives and solvents as mentioned previously. The viscosity and gelation time of the suspensions were measured using an rotational rheometer (Series AR500 TA Instruments, DE, USA). This was carried out using a cone and plate geometry with a 40 mm diameter, cone angle of 2° and gap of 55 μm, rotating against the flat measuring plate. The slurries were pre-sheared for 10 s before measurement by a shear mode with a shear rate in the range 0.1–600 s^{-1} at 22 ℃. The gelation time of the slurries was investigated by measuring the viscosity curves as a function of time after addition of the hardener at a shear rate of 0.1 s^{-1} and 22 ℃. 10 specimens of the green samples and sintered samples with diameters of ~9–12 mm and thickness ~ 1.8–3 mm with ~9 mm and were used to determine the green density by Archimedes' principle. 20 specimens with dimension of 45 mm length × 4 mm width × 3 mm thickness were used to determine the flexural strength with a three-point bending technique. This measurement was carried out using an Instron testing machine (Instron, Buckinghamshire, UK) with a three-point bending technique. All the measurements used a 1 N load cell, a span length of a specimen of 30 mm, and crosshead speed of 1 mm/min. The flexural strength, σ_f, was determined by a equation as shown in a literature [32].

3.3. Fabrication of 1–3 randomised piezocomposites

A generic process of fabricating 1–3 randomised composites using the gel casting method is illustrated in Fig. 1. 3-inch single crystal (<100>) silicon wafers were employed to obtain master mould with randomised pattern (pillar region 2 × 2 mm^2, feature dimensions of 2–50 μm and pillar height of ~170 μm) by deep dry etching process [13,33]. The master mould was adhered on a glass slide (a), followed by surrounding with a (green) Teflon block within a petri dish to form a mould (b) PDMS (Dow Corning Corporation Ltd., UK) was cast into the mould (b), followed by demoulding after curing (d). The PZT suspension was degassed in a vacuum chamber to remove bubbles before casting into the soft PDMS mould (d). The suspension was slowly cast into the soft mould from one corner until fully filled into the mould, in order to minimise air entrapment. After casting, degassing was needed to ensure the suspension was fully filled into the mould cavities. A glass slide was then placed on top to prevent the sample from warping as a result of fast drying (e). The entire assembly was left at room temperature for 48 hr before drying in an oven at 40 °C for another 24 hr to ensure that the sample was completely dried prior to demoulding (f). Careful manual demoulding resulted in samples with ~80% yield of surviving pillars. Before sintering, a burn-out process was employed to remove any additives. This used two temperatures, 250 and 400 °C with a ramp rate of 1 °C/min and dwell time of 1 hr for each temperature to ensure that the polymers were completely decomposed from the sample. The green bristle block (g) was sintered at 1200 °C for 1 hr in a lead oxide rich atmosphere.

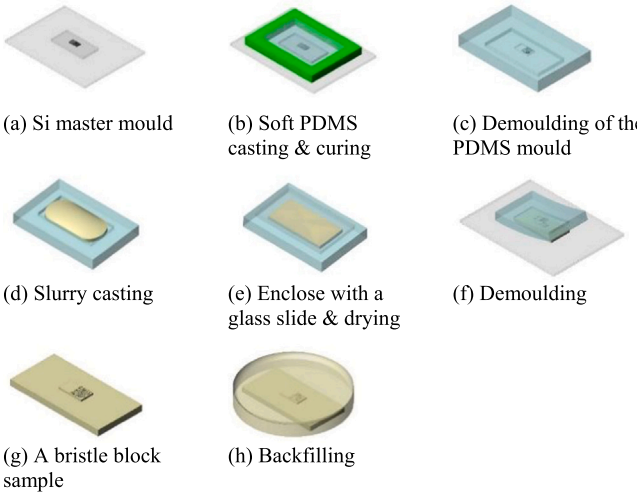

Fig. 1. Illustration of the fabrication process for a 1–3 randomised composite based on a gel casting method.

The sintered sample (h) was encapsulated in a mixture of Epofix resin and hardener (Struers, UK) with a weight ratio of 25:3 g. Prior to encapsulation, the mixture was degassed to remove air bubbles, then it was slowly poured into the sample from one side of the container to prevent air entrapment between the pillars. The assembly was intermittently degassed with a total duration of 20 mins to remove air bubbles. The epoxy was cured in an oven at elevated temperatures 40–60 ℃ with a ramp rate of 1 ℃/min, followed by holding at 60 °C for 3 hr to increase the crosslink density. This was done to enhance the chemical and heat resistance of the epoxy by raising the glass transition temperature of the epoxy [34] so that it would tolerate the relatively harsh environmental conditions in the photolithography process.

3.4. Photolithography for array element microfabrication

Prior to photolithography, the major surfaces of the composite were prepared to be smooth, parallel, and planar for good definition of the ultra-fine array elements. This was done by lapping to expose the ceramic pillars then polishing with a Logitech PM5 lapping machine (Logitech, Glasgow UK), through a process reported elsewhere [35]. The total thickness of the composite with a stock layer was ~1 mm, allowing the composite to withstand high temperatures in the photolithography process.

Photolithography based on a bilayer lift-off process was employed to create a 50-μm pitch electrode array including 20 array elements and fan-out on the composite substrate, with total dimension of 15 × 15 mm^2 and a composite region at the center of 1.3 × 1.3 mm^2 as shown in Fig. 2(a). The first step in the process was to clean the piezocomposite surface with a sponge immersed in IPA solvent. Two types of positive photoresist are needed to create an undercut in the resist profile in the bilayer process. LOR3A (based on polydimethylglutarimide) (Kayaku.

Advanced Materials, MA, USA) was employed as the primary photoresist and spun at 4000 rpm for 30 s to create a thin film on the composite substrate, followed by baking on a hot plate at 150 °C for 5 min. S1818 was then spun at the same spinning condition over the primary resist, followed by baking at 115 °C for 3 min.

The sample was exposed to UV (i-line, 365 nm) through a chromium mask to alter resist solubility then immersed in MIF319 (Metal-Ion-Free) developer (Kayaku Advanced Materials, MA, USA) for 2 min 50 s. The exposed resist was dissolved and the resist profile with the pattern of the arrays was subsequently developed on the substrate. Prior to metal deposition, the surface was cleaned using a plasma etcher (PlasmaFab, 505 Barrel Asher, UK) at 150 W for 1 min to promote adhesion. Metal deposition was carried out using a MEB 550 S electron beam evaporator (PLASSYS Bestek, Marolles-en-Hurepoix, France) under a vacuum,

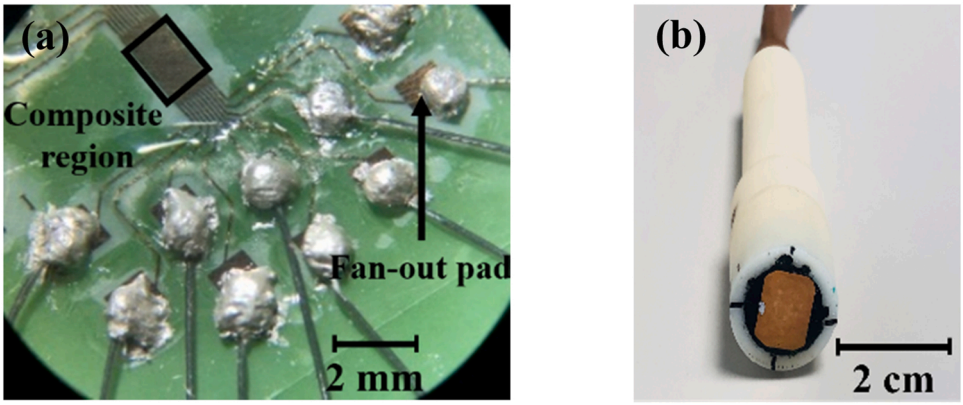

Fig. 2. Photograph of (a) the 1–3 randomised PZT piezocomposite arrays after interconnection and (b) the packaged transducer.

pressure $< 1 \times 10^{-6}$ mbar. Thin films of Ti/Au with a total thickness of 200 nm were deposited on the exposed resist on the composite substrate then lift-off was performed to realize the electrode pattern.

3.5. Electrical impedance spectroscopy

After photolithography, the composite array was lapped to the required thickness of ~ 50 μm by removing material from the major surface opposing the one on which the electrodes were patterned. A ground electrode comprising 200 nm Ti/Au was deposited and poling was performed at 30 kV for 10 min with a bespoke corona poling system (University of Birmingham, Birmingham, UK). This non-contact method was employed to avoid the risk of scratching with a contact poling pin. The electrical impedance magnitude response of each element was measured to assess electrical f_r and mechanical f_a resonances with minimum and maximum magnitudes, respectively, by a 4395 A impedance analyser (Keysight, CA, USA) in a frequency interval 10 Hz - 500 MHz. Effective electromechanical coupling coefficient in rod modes (k_{33}) was calculated from the f_r and f_a as expressed in Eq. 1 [36].

$$k_{33} = \sqrt{\frac{\pi}{2} \bullet \frac{f_r}{f_a} \bullet \tan\left(\frac{\pi}{2} \bullet \frac{f_a - f_r}{f_a}\right)} \quad (1)$$

3.6. Transducer packaging and pulse-echo response measurement

20 micro-coaxial cables were bunched together for insertion through a braided sheath with a diameter of 7 mm. The sheath was used as a ground connection from the array to the connection plug. Each micro-coaxial cable was then connected to a corresponding element pad via silver-loaded conductive epoxy (RS Components, Northants, UK) as shown in Fig. 2(a). The housing was then placed over the array before casting the backing layer. 15 *VF*% tungsten-loaded epoxy was used to support the thin composite and reduce reverberation. The entire assembly was cured at room temperature overnight before packaging into the array housing.

A prototype 1–3 randomised PZT piezocomposite μUS array transducer is shown in Fig. 2(b). After packaging, the array was connected to a Verasonics Vantage 128 High Frequency ultrasound research system (Verasonics, WA, USA) and the pulse-echo response of each element was measured using a 5 mm thick quartz flat as a reflector. As a simple demonstration, the pulse-echo responses of the elements in the array were measured by recording reflections from the quartz flat placed in a water bath, at a distance of 5 mm from the array. Each of the 20 array elements was pulsed with a voltage of 5 V and echo data were measured from it.

4. Results and discussions

4.1. Particle size distribution

Fig. 3 shows the particle size distributions of PZT powder as-received and after vibro-milling in distilled water for different periods. It can be seen that the as-received PZT powder presents a bimodal distribution, with primary and secondary centered powder populations at 2.15 and 15 μm. The density curves for all milled powders show monomodal distributions, Fig. 3, with mean particle sizes of 1.61, 1.44 and 1.22, respectively. The changes in specific surface area (SSA) shown in Table 1 are relatively small since the primary particle size did not change with milling time.

4.2. Rheological behaviour

All suspensions manifested both shear thinning and thickening behaviors as shown in Fig. 4(a). The shear thinning behavior was exhibited at very low shear rates from 0 to 100 s^{-1}, indicating that the suspensions flowed with ordered structure. At higher shear rates, the viscosity, η, tended to gradually arise when the shear rate, $\dot{\gamma}$, was increased from 100 to 600 s^{-1}. This behaviour implies that flocculation might gradually form during flow, as the suspension structure changes to a less ordered structure. Nevertheless, η for the two suspensions made with powders milled at 24 and 36 hrs was still lower than 1 Pa.s at the highest shear rate of 600 s^{-1}.

Meanwhile the shear thickening behaviour was accentuated in the

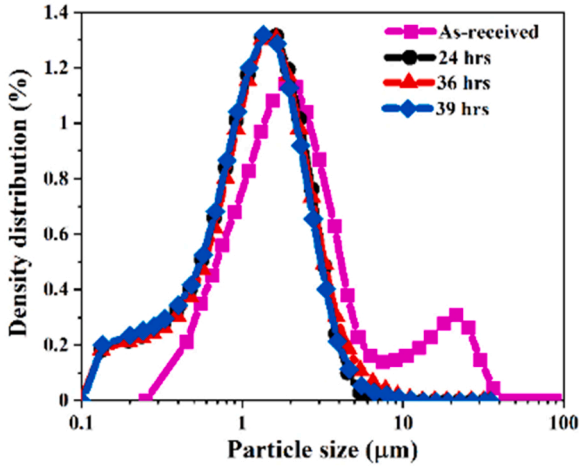

Fig. 3. Particle size distribution curves of PZT powder as-received and milled for 24, 36 and 39 hr.

Table 1
Summary of mean particle size and SSA of the starting and milled PZT powders, and rheological behaviour of each suspension.

PZT powder	Mean Particle Size (μm)	SSA (m^2/g)	Viscosity* (Pa.s)	Gelation time (mins)
As received	8.57	n/a	n/a	n/a
VB – 24 hr	1.61	1.81	0.34	14
VB – 36 hr	1.44	2.16	0.34	12
VB – 39 hr	1.22	2.09	0.47	11

* At shear rate of 100 s^{-1}

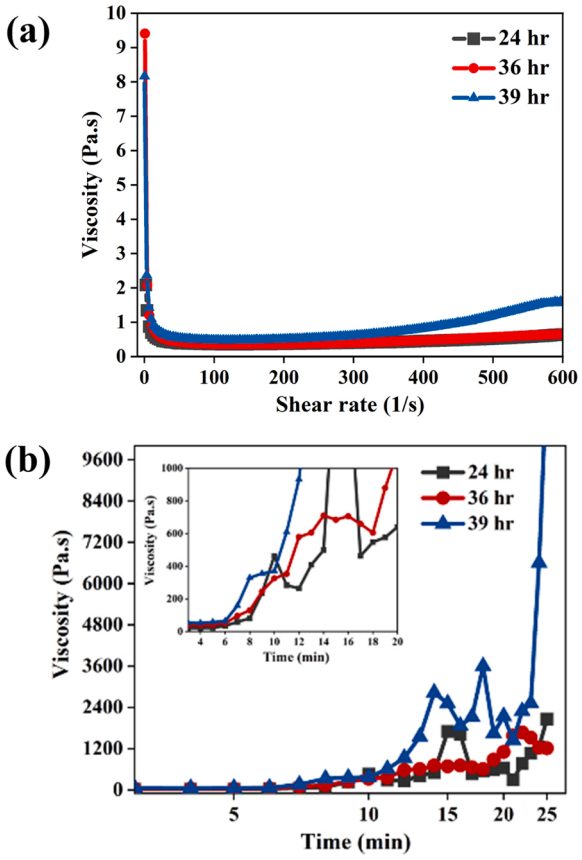

Fig. 4. Variation of viscosity curves for suspensions as (a) a function of shear rate (no hardener addition) and (b) a function of time after addition hardener.

suspension made with powder milled for 39 hr, by showing η of ~1.5 Pa.s at the highest rate. This higher viscosity implies a resistance to the flow of the suspension, which might be attributed to the formation of flocculation caused by cooperation of the finest particles in the powder milled for 39 hr, as listed in Table 1. For this reason, more external force was needed to break the interparticle forces of the flocculation, resulting in higher viscosity and shear thickening behaviour found in this suspension, as also shown elsewhere [30,37–39].

Suspension viscosity is usually considered at a low shear rate of 100 s^{-1} because this is close to the condition during casting [30,40,41]. Hence the suspension made with the powder milled for 39 hr, with the highest viscosity, was still acceptable. Besides, all slurries exhibited low η, < 1 Pa.s, at the low shear rate of 100 s^{-1} as listed in Table 1, indicating that the suspensions had good flowability to fill the mould cavities, as required for gel casting [28,42]. Interestingly, the slurry made with powder milled for 39 hr had higher viscosity, 0.47 Pa.s, than the other two powders. This is attributed to the influence of the finer particles that tend to produce flocculation, which need more energy to push the slurry to flow, leading to high viscosity as described previously.

Fig. 4(b) shows the viscosity curves as a function of time, from which the gelation time of the suspensions can be identified. The start time was counted after the slurries were manually mixed with the hardener, in a process which lasted for approximately 3 min. All suspensions showed a period of constant viscosity, following which their viscosities rose gradually and then increased abruptly towards infinity, representing hardening of the suspension. The period of constant viscosity is known as the gelation time of the polymerisation process, which is the time available for mixing and casting [43]. It was found that all slurries had a period of constant viscosity exceeding 10 min, as presented in Table 1. This indicates that the gelation time of all the slurries was suitable for gel casting, in agreement with the literature [30,43].

The gelation time decreased as the mean particle size was decreased. It is claimed that gelation time reduction is strongly influenced by a 'container' effect [43,44], in which particle interstices acts as containers in the gel system. For slurry gelation, polymer chain lines are needed to simultaneously connect the particles and fill their interstices at a certain period, with the interstices thus acting as a container in the gelling system. The smaller the container, defined as shorter distance between particles, the shorter the polymer chain needed to connect the particles. Olhero and Ferreira [38] suggested that smaller interstices were found in finer particle sizes because of a higher number of particles compared to larger particles in the same volume. For this reason, by reducing the particle size, the container is reduced, resulting in a decrease in gelation time.

4.3. Characterisation of green and sintered samples

Because the smallest feature size in the randomised pillar pattern was 2 μm, Fig. 4, the milled powder with mean particle size 1.22 μm, corresponding to the 39 hr milling time, was chosen for further processes, to prevent particle blocking of the mould. Bulk and bar samples obtained green density and green strength and sintered density of 4.79 ± 0.11 g/cm^3, 49.7 ± 2.49 MPa, and 7.5 ± 0.62 g/cm^3, respectively. It was noticed that the green strength obtained in this work improved significantly compared to the previous work by Jiang et al. (~38 MPa), who fabricated 1–3 randomised composites by using EGDGE resin with the gel casting method [24]. This might be attributed to better water solubility of the hydantoin resin [28], to which a higher solid loading of 48 vol% could be added while maintaining a low viscosity level. In comparison with the work of Jiang et al., the suspension made with 45 vol% solid loading and 30 wt% EGDGE resin had the viscosity of 1.23 Pa.s at a shear rate of 100 s^{-1}.

Fig. 5. shows the microstructure of the bulk and pillars. Open pores were obviously seen in the green sample surfaces owing to solvent evaporation as illustrated in Fig. 5(a). The microstructure of the surface of sintered samples (Fig. 5(c)) showed a grain size of around 1–2 μm. Micropores were observed in the fracture surfaces of the sintered sample (Fig. 5(d)), which were affected by decomposition of the high resin content [30,33]. The sintered bristle block sample shrank by 35% with dimension measured at pillar region of 1.3 × 1.3 mm^2.

The finest feature size is ~ 2 μm and the height of the pillars is ~124 μm, providing *AR* up to 62. The microstructure (Fig. 5(e-f)) shows a homogenous and uniform grain size as well as shape integrity, showing that the suspension completely filled the mould cavities. Some tilted pillars were observed in the sintered samples; these may have occurred during the sintering process.

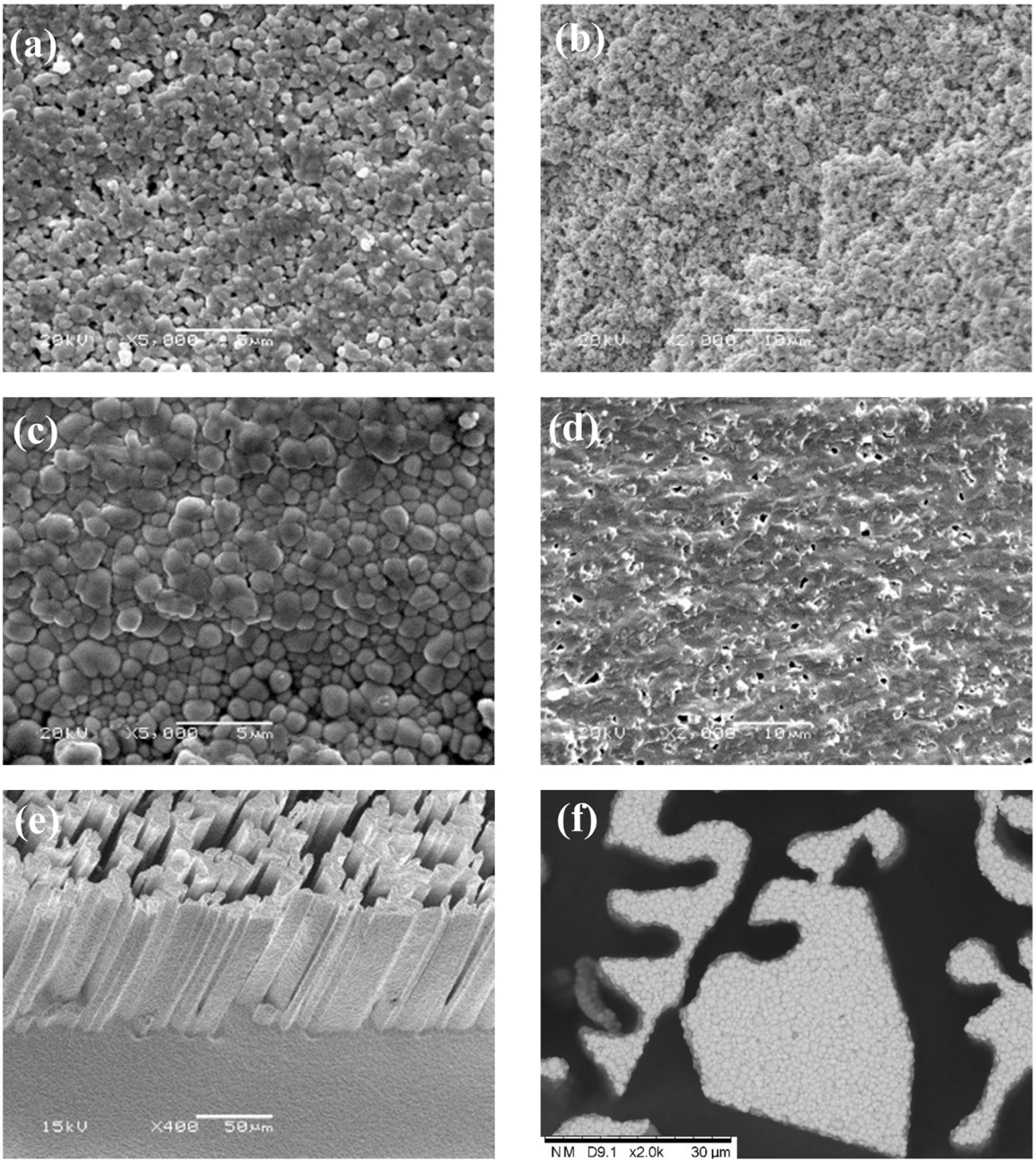

Fig. 5. SEM images of surface and fracture of (a-b) green sample (c-d) sintered sample and sintered random ceramic structure; (a) detailed view at 50°, and (b) detailed top view.

4.4. Surface profile

Fig. 6(a) shows 3D optically profiled images of the piezocomposite surface after pillar exposure via a final lapping process with 3-µm Al_2O_3 abrasive. Each color represents the height of the spot. Epoxy bumps are present in the composite surface due to the dissimilarity in the elastic characteristics of the two materials in the composite [45,46]. An average surface roughness (R_a) of the randomised piezocomposite measured by the optical profiler was around 23.21 ± 2.71 nm. Fig. 6(b) shows the microstructure of a 1–3 randomised piezocomposite, the gap where a grain has pulled out and a pinhole. The grain pull-out may have been caused by chipping during the lapping process [46] and the pinhole is likely to have originated from bubble entrapment by defects in the polymer.

In the composite fabrication, vacuum degassing and the use of a centrifuge and heat are generally recommended as efficient methods to remove air bubbles from the epoxy before curing [47]. The presence of pinholes indicates that the pressure and elapsed time during degassing might not have been sufficient to force the bubbles to exit through the liquid epoxy. In addition, curing at elevated temperatures also assists bubble removal by lowering the viscosity of the epoxy mixture, allowing the bubbles to flow up to the surface of the mixture. However, this method comes at the expense of shortened pot life and limited time for bubble removal [47,48], which might cause the bubbles to become trapped within the structure.

4.5. 50-µm pitch array elements patterned on a 1–3 randomised piezocomposite

The photolithography process based on bilayer lift-off was developed

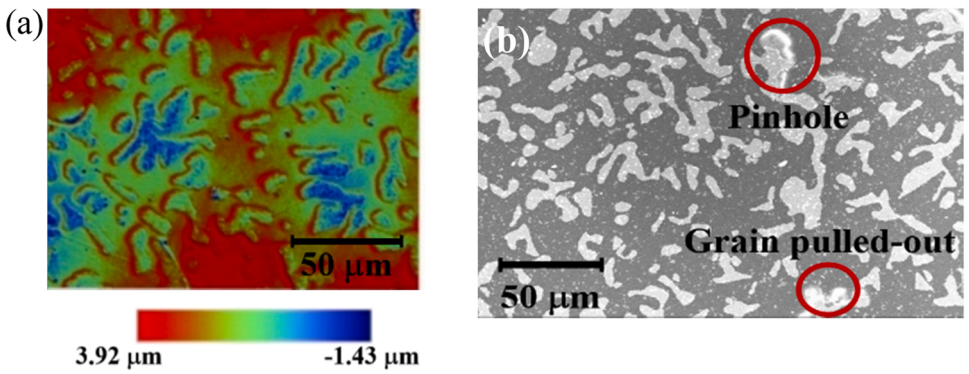

Fig. 6. (a) A three-dimensional optically profiled image showing height variation on a composite surface and (b) a SEM image of 1–3 randomised ceramic composite showing ceramic pillars (white region) embedded in epoxy (black region) and defects in the piezocomposite.

to deposit and pattern the electrodes of the array elements with an element pitch of 50-μm, i.e., 35-μm trace and 15-μm kerf, on the top surface of the piezocomposite as shown in Fig. 7. Shape deformation at edges of the traces was noticed when the electrodes were patterned on the composite region as shown in Fig. 7(b). This is because the element shape varied along with the irregularly- shaped pillars. However, traces with an average width of 34.4 ± 0.17 μm were achieved on the composite surface.

4.6. Electrical impedance characteristics

Fig. 8(a)-(b) show the electrical impedance magnitude and phase measured from the 20 elements in the piezocomposite array. The functional elements showed indications of the f_r and f_a resonances, representing typical characteristics of impedance magnitude spectra. The magnitude characteristics of elements 1 and 12, which are featureless and high magnitude, imply inactive elements (Fig. 8(c)), likely caused by electrical short-circuits through pinholes during poling (visible in Fig. 6(b)). Thus, the number of working elements in the composite array was 18, from a total of 20 elements. In addition, the discrepancies in impedance magnitude and $k_{33,}$ as illustrated in Fig. 8(a) - 9, are attributed to the variation in the effective volume of piezoelectric material beneath the element [49].

The electrical impedance characteristics of the elements in the piezocomposite array show no significant spurious modes within a wide range of frequencies, indicating that the unwanted modes are eliminated from the thickness resonance, in agreement with the literature [24,30],. Influential factors are the random distribution of pillar geometry and spacing and the relatively high *AR* in the range ~1–25, calculated from the composite thickness of 50 μm. In the repetitive and symmetrical structure of a classic 1–3 composite with square pillars, spurious modes arise from waves propagated laterally between pillars and reflected at the parallel pillar faces within the composite structure [4]. The random geometry and distribution of the pillars scatters the reflected waves because the periodicity of the pillars no longer exists and because the pillar surfaces are not parallel anymore. In addition, the high *AR* in the randomised piezocomposite enhances the thickness resonance frequencies, which become dominant over the spurious modes [4,6], providing a mean k_{33} of 0.67 (Fig. 9).

4.7. Pulse-echo response

Fig. 10(a)-(b) shows pulse-echo data and frequency bandwidth of element 10 in the 1–3 randomised piezocomposite μUS array. This element had the centre frequency (f_C) of 32 MHz, − 6 dB fractional bandwidth (BW) of 32.6%, and a − 20 dB pulse length (*PL)* of 0.29 μs. The variations of f_C and BW between elements are presented in Fig. 10 (c). These variations are attributed to the diversity in the effective volume of the piezoelectric material beneath each element; whilst the overall average ceramic volume fraction is 40%, there may be some variation between elements due to the random distribution of the ceramic pillars themselves. Mean f_C and BW were found to be 27.1 ± 3.5 MHz, and 38.4 ± 17.4%, respectively. It is well known that a *PL* is inversely proportional to BW [50]. Thus, an element with shorter *PL* provides broader BW. In the present piezocomposite array, the *PL* is relatively large compared with other work [51,52], with mean value of 0.26 μs, providing maximum axial resolution (R_A) of 200 μm. However, the present array lacks an acoustic matching layer and matching of its electrical impedance to the driving electronics [53,54]. Additionally, the total volume fraction of piezoceramic within the piezocomposite could be adjusted, as could be the acoustic impedance of the backing layer to optimize the performance for any specific application. The pulse-echo results nevertheless prove the validity of 1–3 randomised piezocomposite as a route towards wafer-scale development of μUS linear arrays.

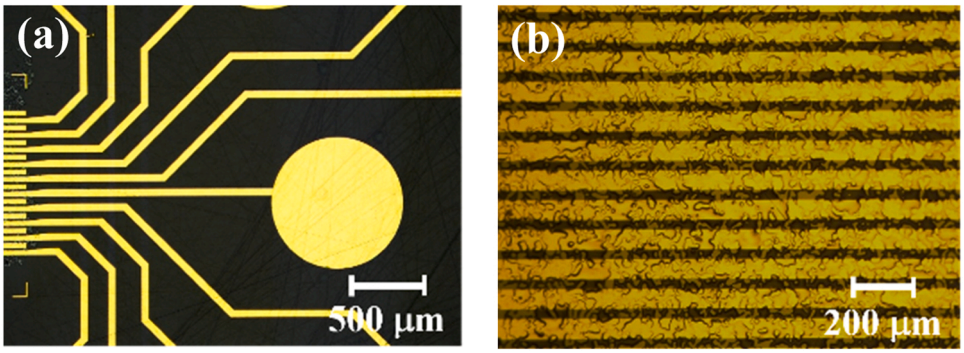

Fig. 7. Photomicrographs of deposited metals (Ti/Au) on surfaces of 1–3 randomised PZT piezocomposites.

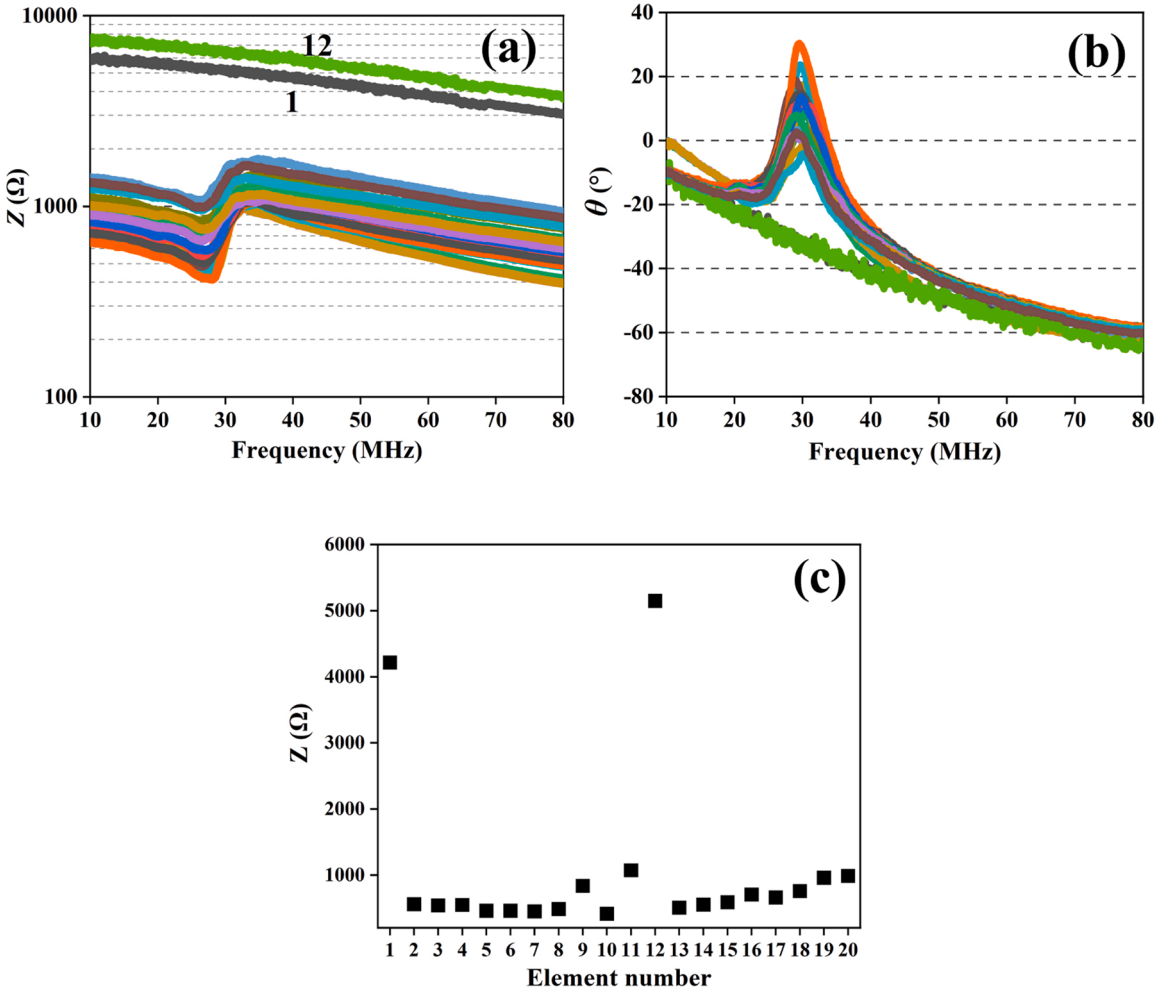

Fig. 8. (a) Electrical impedance magnitude (Z),(b) phase (θ), and (c) electrical impedance magnitude at the resonance frequency for 20 elements in 1–3 randomised PZT piezocomposite array.

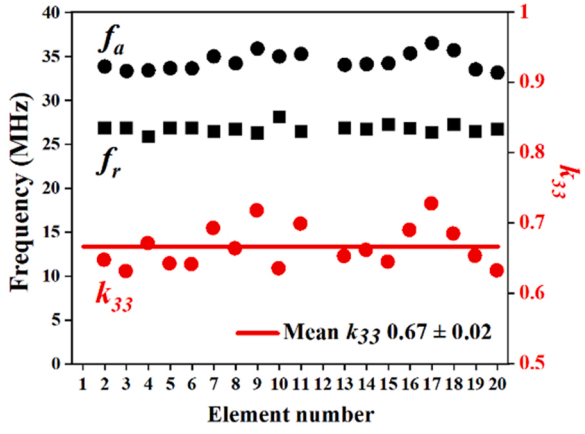

Fig. 9. Electrical f_r and mechanical f_a resonance frequencies and calculated k_{33} for all elements.

5. Conclusions

This paper addressed a new manufacturing process based on gel casting associated with micromoulding for fabrication of novel 1–3 randomised piezocomposites as the basis for μUS linear arrays. Under the optimal condition of 48 vol% solid loading and 30 wt% hydantoin resin content, the viscosities of the suspension increased with respect to the mean particle size. All suspensions showed both shear thinning and thickening behaviors. The shear thickening behaviour was more accentuated in the suspension made with the finest powder of 1.22 μm, showing $\eta \sim 1.5$ Pa.s at the highest rate at 600 s^{-1}. However, its viscosity measured at a shear rate of 100 s^{-1} remained lower than 1 Pa.s, still representing good flowability of the suspension.

Bristle block samples were achieved with high shape integrity, green strength of 48 MPa, and *AR* up to 62, measured after sintering, all these characteristics being beneficial for subsequent processing. A prototype 20 element μUS array was produced to demonstrate the capability to reduce spurious modes and obtain high $k_{33} = 0.67$. The array provided mean − 6 dB bandwidth of 38.4% and pulse length of 0.26 μs, suggesting axial resolution of 200 μm. Thus, the gel casting associated with micromoulding shows its feasibility as an alternative and cost-effective method in producing the irregular-shaped pillars with high shape integrity, high pillar aspect ratio for 1–3 piezocomposite high frequency ultrasound array. Although, the 1–3 randomised piezocomposite array had poor acoustic properties, but it remained functionality and demonstrated its capability in reducing the spurious modes from the fundamental modes. Besides, this alternative method also has the potential for wafer-scale fabrication simply through the use of larger moulds.

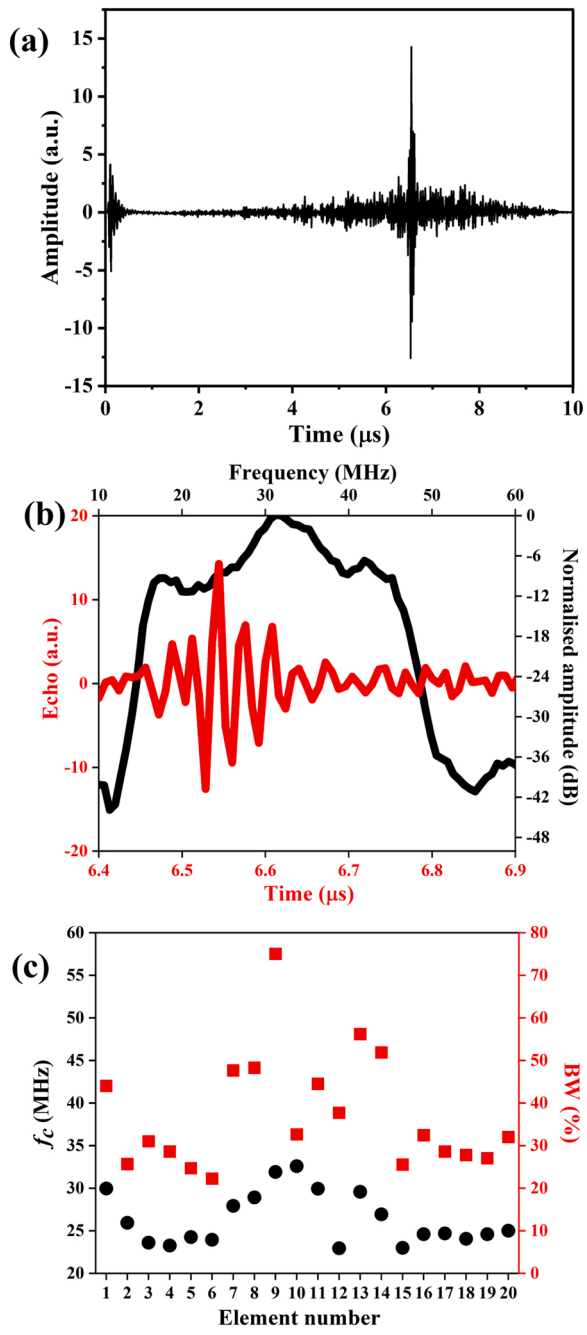

Fig. 10. (a) Pulse-echo signals of element 10, (b) Echo response and bandwidth of element 10 (c) Calculated centre frequency (f_c) and − 6 dB fractional bandwidth for all elements in the 1–3 randomised PZT piezocomposite μUS array.

Declaration of Competing Interest

The authors declare that they have no known competing financial interests or personal relationships that could have appeared to influence the work reported in this paper.

Acknowledgements

A. Boonruang is supported by Royal Thai Government Scholarships and TISTR (Pathum Thani, Thailand). The authors also acknowledge the James Watt Nanofabrication Centre, University of Glasgow for clean room facilities and the support of the EPSRC Sonopill Programme (grant number EP/K034537). The authors are also grateful to the JECS Trust for funding from the Piezo 2021 School and Conference for the article publication charge (Contract No. 2019219).

References

[1] K. Uchino, Advanced Piezoelectric Materials, Woodhead Publishing, 2010, https://doi.org/10.1533/9781845699758.
[2] W.A. Smith, A. Shaulov, B.A. Auld, Tailoring the Properties of Composite Piezoelectric Materials for Medical Ultrasonic Transducers *Ultrason Symp. Proc.* Publ. Online, 1985, pp. 642–647 doi: 10.1109/ultsym.1985.198589.
[3] A. Safari, V.F. Janas, A. Bandyopadhyay, Development of fine-scale piezoelectric composites for transducers, J. Ceram. Process. 43 (11) (1997) 2849–2856, https://doi.org/10.1002/aic.690431334.
[4] W.A. Smith, B.A. Auld, Modeling 1–3 composite piezoelectrics: thickness-mode oscillations, IEEE Trans. Ultrason. Ferroelectr. Freq. Control 38 (1) (1991) 40–47, https://doi.org/10.1109/58.67833.
[5] J. Yin, M. Lee, J. Brown, E. Chérin, F.S. Foster, Effect of triangular pillar geometry on high- frequency piezocomposite transducers, IEEE Trans. Ultrason. Ferroelectr. Freq. Control 57 (4) (2010).
[6] G. Hayward, J. Bennett, R. Hamilton, A theoretical study on the influence of some constituent material properties on the behavior of 1-3 connectivity composite transducers, J. Acoust. Soc. Am. 98 (4) (1995) 2187–2196, https://doi.org/10.1121/1.413333.
[7] W.D. Callister, in: J. Hayton (Ed.), Materials Science and Engineering, John Wiley & Sons, Inc, 2007.
[8] J.A. Brown, F.S. Foster, A. Needles, E. Cherin, G.R. Lockwood, Fabrication and performance of a 40-MHz linear array based on a 1-3 composite with geometric elevation focusing, IEEE Trans. Ultrason. Ferroelectr. Freq. Control 54 (9) (2007) 1888–1894, https://doi.org/10.1109/TUFFC.2007.473.
[9] H.J. Lee, S. Zhang, Y. Bar-Cohen, S. Sherrit, High temperature, high power piezoelectric composite transducers, Sensors 14 (8) (2014) 14526–14552, https://doi.org/10.3390/s140814526.
[10] J.A. Brown, E. Chérin, J. Yin, F. Stuart Foster, Fabrication and performance of high-frequency composite transducers with triangular-pillar geometry, IEEE Trans. Ultrason. Ferroelectr. Freq. Control 56 (4) (2009) 827–836, https://doi.org/10.1109/TUFFC.2009.1106.
[11] Jianhua Yin, M. Lee, E. Cherin, M. Lukacs, Foster, FS. High-frequency piezo-composite transducer with hexagonal pillars. *IEEE Int Ultrason Symp*. Published online 2009. doi:⟨10.1109/ULTSYM.2009.5441815⟩.
[12] H.C. Yang, J. Cannata, J. Williams, K. Shung, Crosstalk reduction for high-frequency linear-array ultrasound transducers using 1-3 piezocomposites with pseudo-random pillars, IEEE Trans. Ultrason Ferroelectr. Freq. Control 59 (10) (2012) 2312–2321, https://doi.org/10.1109/TUFFC.2012.2456.
[13] 1–3 C.E.M. Demore, S. Cochran, L. Garcia-Gancedo, F. Dauchy, T.W. Button, J.C. Bamber, Piezocomposite design optimised for high frequency kerfless transducer arrays. *Proc - IEEE Ultrason Symp*. Published online 2009. doi:⟨10.1109/ULTSYM.2009.5442007⟩.
[14] L.J. Bowen, R.L. Gentilman, H.T. Pham, D.F. Fiore, K.W. French, Transducers 1993 Ultrasonics Symposium. Published online 1993:499–504.
[15] B.G. Pazol, L.J. Bowen, R.L. Gentilman, et al., Ultrafine scale piezoelectric composite materials for high frequency ultrasonic imaging arrays, Proc. IEEE Ultrason Symp. 2 (1995) 1263–1268, https://doi.org/10.1109/ultsym.1995.495787.
[16] R. Liu, K.A. Harasiewicz, F. Stuart Foster, Interdigital pair bonding for high frequency (20–50 MHz) ultrasonic composite transducers, IEEE Trans. Ultrason Ferroelectr. Freq. Control 48 (1) (2001) 299–306, https://doi.org/10.1109/58.896143.
[17] H.R. Chabok, J.M. Cannata, H.H. Kim, J.A. Williams, J. Park, K.K. Shung, A high-frequency annular-array transducer using an interdigital bonded 1-3 composite, IEEE Trans. Ultrason Ferroelectr. Freq. Control 58 (1) (2011) 206–214, https://doi.org/10.1109/TUFFC.2011.1787.
[18] M. Lukacs, J. Yin, G. Pang, et al., Performance and characterization of high frequency linear arrays, Proc. - IEEE Ultrason Symp. 1 (10) (2005) 105–108, https://doi.org/10.1109/ULTSYM.2005.1602807.
[19] F.S. Foster, J. Mehi, M. Lukacs, et al., A New 15–50 MHz array-based micro-ultrasound scanner for preclinical imaging, Ultrasound Med Biol. 35 (10) (2009) 1700–1708, https://doi.org/10.1016/j.ultrasmedbio.2009.04.012.
[20] K.A. Snook, C.H. Hu, T.R. Shrout, K.K. Shung, High-frequency ultrasound annular-array imaging. Part I: array design and fabrication, IEEE Trans. Ultrason. Ferroelectr. Freq. Control 53 (2) (2006) 300–308, https://doi.org/10.1109/TUFFC.2006.1593368.
[21] S. Wang, J.F. Li, K. Wakabayashi, M. Esashi, R. Watanabe, Lost silicon mold process for PZT microstructures, Adv. Mater. 11 (10) (1999) 873–876, https://doi.org/10.1002/(SICI)1521-4095(199907)11:10<873::AID-ADMA873>3.0.CO;2-F.
[22] T.J. Clipsham, T.W. Button, 1-3 Piezocomposites realised from small feature size, high aspect ratio, hot embossed moulds. Part II: piezocomposite fabrication, Microsyst. Technol. 16 (11) (2010) 1983–1988, https://doi.org/10.1007/s00542-010-1132-7.
[23] S. Cochran, A. Abrar, K.J. Kirk, et al., Net-shape ceramic processing as a route to ultrafine scale 1-3 connectivity piezoelectric ceramic-polymer composite transducers (c): Proc. - IEEE Ultrason Symp. 3 (2004) 1682–1685, https://doi.org/10.1109/ULTSYM.2004.1418147.

[24] Y. Jiang, C.E.M. Demore, C. Meggs et al. Micro-moulded randomised piezocomposites for high frequency ultrasound imaging. *IEEE Int Ultrason Symp IUS*. Published online 2012:4–7. doi:⟨10.1109/ULTSYM.2012.0045⟩.
[25] O.O. Omatete, M.A. Janney, S.D. Nunn, Gelcasting: from laboratory development toward industrial production, J. Eur. Ceram. Soc. 17 (2–3) (1997) 407–413, https://doi.org/10.1016/s0955-2219(96)00147-1.
[26] O.O. Omatere, Data RUSA, Precision F, From S, Derrington PE, Ivan L. METHOD FORMOLDING CERAMIC POWDERS USING AWATER-BASED GEL CASTING. 1991; (19).
[27] J.S. Ha, Effect of atmosphere type on gelcasting behavior of Al2O3 and evaluation of green strength, Ceram. Int 26 (3) (2000) 251–254, https://doi.org/10.1016/S0272-8842(99)00050-4.
[28] R. Xie, D. Zhang, X. Zhang, K. Zhou, T.W. Button, Gelcasting of alumina ceramics with improved green strength, Ceram. Int 38 (8) (2012) 6923–6926, https://doi.org/10.1016/j.ceramint.2012.05.027.
[29] X. Mao, S. Shimai, M. Dong, S. Wang, Gelcasting of alumina using epoxy resin as a gelling agent, J. Am. Ceram. Soc. 90 (3) (2007) 986–988, https://doi.org/10.1111/j.1551-2916.2007.01492.x.
[30] T. Thongchai, Fabrication of Lead Free and Lead Based 1–3 Piezoelectric Composites for High Frequency Ultrasound Transducers. 2017;(September). ⟨https://etheses.bham.ac.uk/id/eprint/8041/⟩.
[31] B. Su, D.H. Pearce, T.W. Button, Routes to net shape electroceramic devices and thick films, J. Eur. Ceram. Soc. 21 (10–11) (2001) 2005–2009, https://doi.org/10.1016/S0955-2219(01)00161-3.
[32] M.Y. Tsai, P.S. Huang, J.H. Yeh, et al., Evaluation of three-point bending strength of thin silicon die with a consideration of geometric nonlinearity, IEEE Trans. Device Mater. Reliab 19 (4) (2019) 615–621, https://doi.org/10.1109/TDMR.2019.2937988.
[33]] Y. Jiang, Fabrication and characterisation of novel ultrasound transducers. 2013; (April). ⟨http://etheses.bham.ac.uk/id/eprint/4401⟩.
[34] *E.M., Petrie, Epoxy Adhesive Formulations*. (Edward M. Petrie, ed.). The McGraw-Hill Companies; 2006. ⟨http://books.google.fr/books?id=738MPfO5FEkC⟩.
[35] A. Boonruang, T. Thongchai, T. Button, S. Cochran, Microfabrication of 1–3 Composites with Photolithographically Defined Electrode Patterns for Kerfless Microultrasound Arrays. In: *IEEE International Ultrasonics Symposium, IUS*. Vol 2019-Octob.; 2019:1746–1749. doi:⟨10.1109/ULTSYM.2019.8925545⟩.
[36] Publication and Proposed Revision of ANSI/IEEE Standard 176-1987 'ANSI/IEEE Standard on Piezoelectricity IEEE Trans. Ultrason Ferroelectr. Freq. Control 43 5 1996 717 doi: 10.1109/TUFFC.1996.535477.
[37] X. Xu, Z. Wen, X. Wu, J. Lin, X. Wang, Rheology and chemorheology of aqueous γ-$LiAlO_2$ slurries for gel-casting, Ceram. Int 35 (6) (2009) 2191–2195, https://doi.org/10.1016/j.ceramint.2008.11.033.
[38] S.M. Olhero, J.M.F. Ferreira, Influence of particle size distribution on rheology and particle packing of silica-based suspensions, Powder Technol. 139 (1) (2004) 69–75, https://doi.org/10.1016/j.powtec.2003.10.004.
[39] R. Hoffman, Explanations for the cause of shear thickening in concentrated colloidal suspensions, J. Rheol. 42 (1) (1998) 111–123, https://doi.org/10.1122/1.550884.
[40] R. Xie, C. Liu, Y. Zhao, P. Jin, KechaoZhou, D. Zhang, Gelation behavior and mechanical properties of gelcast lead zirconate titanate ceramics, J. Eur. Ceram. Soc. 35 (7) (2015) 2051–2056, https://doi.org/10.1016/j.jeurceramsoc.2015.01.009.
[41] R. Xie, Y. Zhao, K. Zhou, D. Zhang, Y. Wang, H.L.W. Chan, Fabrication of fine-scale 1-3 piezoelectric arrays by aqueous gelcasting, J. Am. Ceram. Soc. 97 (8) (2014) 2590–2595, https://doi.org/10.1111/jace.13001.
[42] C. Jiang, X. Gan, D. Zhang, R. Xie, K. Zhou, Gelcasting of aluminum nitride ceramics using hydantion epoxy resin as gelling agent, Ceram. Int 39 (8) (2013) 9429–9433, https://doi.org/10.1016/j.ceramint.2013.05.060.
[43] G. Liu, M.M. Attallah, Y. Jiang, T.W. Button, Rheological characterization and shape control in gel-casting of nano-sized zirconia powders, Ceram. Int. 40 (9) (2014) 14405–14412, https://doi.org/10.1016/j.ceramint.2014.06.036.
[44] M. Dong, X. Mao, Z. Zhang, Q. Liu, Gelcasting of SiC using epoxy resin as gel former, Ceram. Int. 35 (4) (2009) 1363–1366, https://doi.org/10.1016/j.ceramint.2008.07.008.
[45] MacLennan D. Fundamental Characterisation and Early Functional Testing of Micromoulded Piezocomposites. Published online 2010:1–264.
[46] Bernassau A. Micro-Engineering for High Frequency Ultrasound Arrays. 2009; (May).
[47]] Epoxy Technology. *Removing Bubbles from Epoxy*.; 2009. ⟨www.epotek.com⟩.
[48] M. Afendi, W.M. Banks, D. Kirkwood, Bubble free resin for infusion process, Compos Part A Appl. Sci. Manuf. 36 (6) (2005) 739–746, https://doi.org/10.1016/j.compositesa.2004.10.030.
[49] Youngqiang Q. Development of Ultrasonic Devices for Microparticle and Cell Manipulation. 2014;(June).
[50] T.A. Whittingham, Broadband Transducers, Eur. Radio. 3 (1999) 298–303.
[51] J.M. Cannata, J.A. Williams, Q. Zhou, T.A. Ritter, K. Kirk Shung, Development of a 35-MHz piezo-composite ultrasound array for medical imaging, IEEE Trans. Ultrason Ferroelectr. Freq. Control 53 (1) (2006) 224–235, https://doi.org/10.1109/TUFFC.2006.1588408.
[52] T.A. Ritter, T.R. Shrout, R. Tutwiler, K.K. Shung, A 30-MHz piezo-composite ultrasound array for medical imaging applications, IEEE Trans. Ultrason. Ferroelectr. Freq. Control 49 (2) (2002) 217–230, https://doi.org/10.1109/58.985706.
[53] X. Jian, Z. Li, Z. Han, et al., The study of cable effect on high-frequency ultrasound transducer performance, IEEE Sens J. 18 (13) (2018) 5265–5271, https://doi.org/10.1109/JSEN.2018.2838142.
[54] Y. Yang, X. Wei, L. Zhang, W. Yao, The effect of electrical impedance matching on the electromechanical characteristics of sandwiched piezoelectric ultrasonic transducers, Sensors (12) (2017) 17, https://doi.org/10.3390/s17122832.